Supplementary Information for

Propagation of spike timing and firing rate in feedforward networks reconstituted *in vitro*

Jérémie Barral, Xiao-Jing Wang, and Alex Reyes

Supplementary Figures 1 to 8

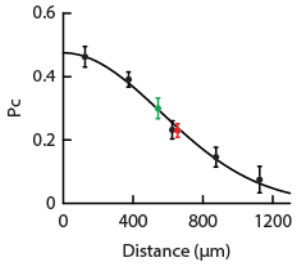

Supplementary Figure 1: Connectivity in feedforward networks.

Probability of connection within a given layer (green; $P_c = 0.3 \pm 0.06$; mean ± SEM; n = 50 tested connections; 533 ± 132 µm apart; mean ± SD) or between two adjacent layers (red; $P_c = 0.23 \pm 0.04$, mean ± SEM; n = 100 tested connections; 666 ± 140 µm apart; mean ± SD). Also shown is the probability of connection that was measured in random recurrent networks of neurons in culture and the corresponding Gaussian fit (data from (Barral and Reyes 2016)). The data shows that connection probability did not depend on the architecture of the network and was readily predicted from the interneuronal distance. Data presented as mean ± SEM.

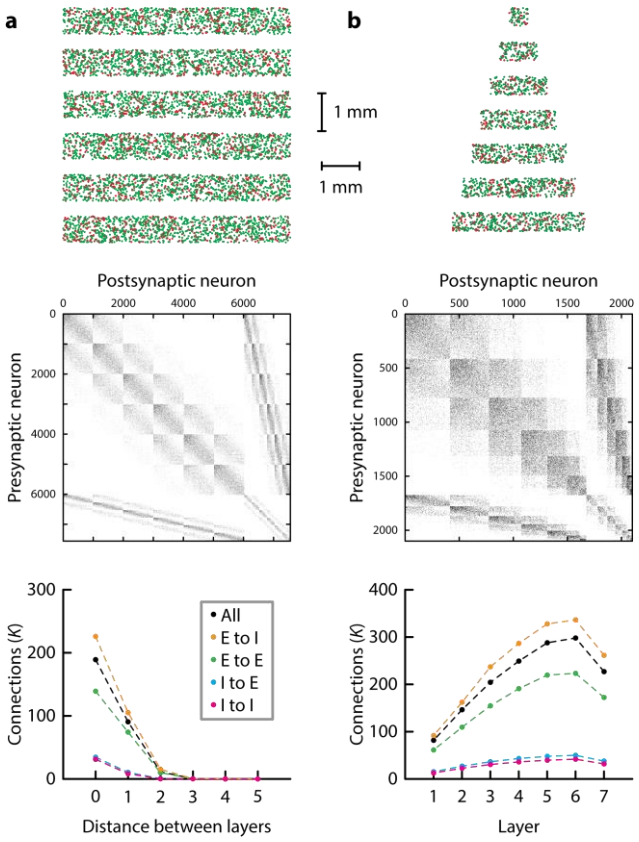

Supplementary Figure 2: Simulation of connectivity in modular networks.

We used simulations to compute the connectivity in feedforward networks made of layers of same size (**a**) or of different size (**b**). Top: schematic of the feedforward network. Excitatory (green, 80%) and inhibitory (red, 20%) neurons were placed randomly in delimitated chambers (**a**: length: 4 mm, width: 0.7 mm, spacing: 0.4 mm; **b**: length: [0.5 : 0.5 : 35] mm, width: 0.5 mm, spacing: 0.4 mm). The density was 300 neurons/mm^2. Middle: we computed the connectivity matrix based on the following connection profiles: $P_c(x) = p_0 \cdot \exp(-x^2/2\sigma^2)$, where x is the distance between neurons and p_0 and σ were derived from experimental measures using dual patch-clamp recordings (*E-E*: p_0 = 0.4 and σ = 0.9 mm; *E-I*: p_0 = 0.6 and σ = 0.9 mm; *I-E*: p_0 = 0.6 and σ = 0.63 mm; *I-I*: p_0 = 0.5 and σ = 0.63 mm) (Barral and Reyes 2016). Neurons were sorted by 1) their type (excitatory or inhibitory), 2) the layer they belong to, and 3) their position with respect to the center of the layer. Bottom: number of incoming connections *K* depended on its type and on the type of presynaptic neuron. The number of incoming connections was plotted as a function of the distance that separated neurons (**a**) or as a function of the position of the postsynaptic neuron in the network (**b**).

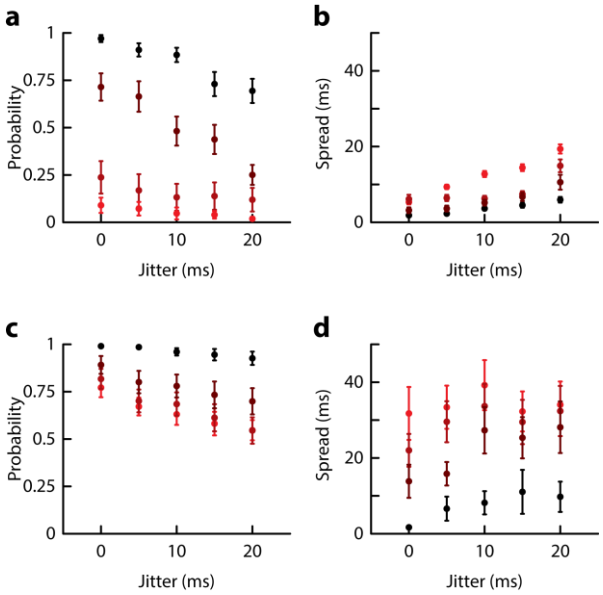

Supplementary Figure 3: Propagation of pulse packets in feedforward networks.

a. Spike probability as a function of jitter in the stimulating pulse packet for different layers in sparse networks (layer 1 to layer 4, from black to red respectively). The spike probability was defined as the probability to evoke at least 1 spike in the 0.5 ms following the stimulation. **b.** Spike delay as a function of jitter in sparse networks. **c.** Same as in **a** but in dense networks. **c.** Same as in **b** but in dense networks. Data are the same as in Fig. 2-3 and are presented as mean ± SEM.

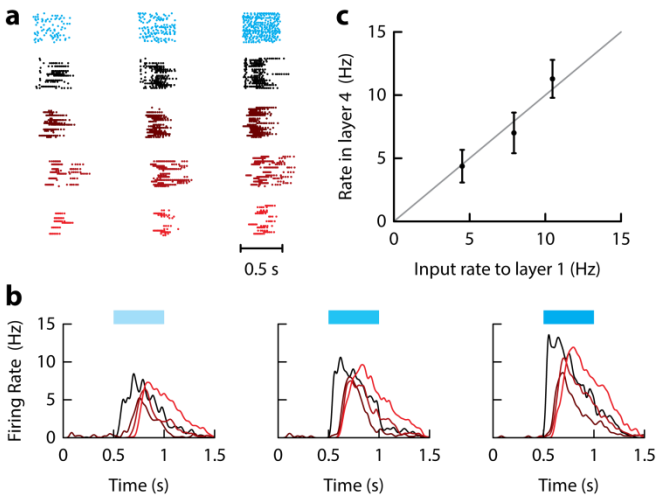

Supplementary Figure 4: Modulation of firing rate by the input firing rate.

a. Raster plot showing the 0.5 s-long Poisson trains of light pulses to the first layer with effective pulse rates of 5, 10, and 20 Hz (blue). Below are shown the responses of neurons in layer 1 to 4 (from black to red, respectively). **b.** Average firing rate of 5 different networks for the 3 different input frequencies. **c.** Output firing rate in layer 4 vs firing rate of the delivered Poisson input the first layer. The original input rate (5, 10, and 20 Hz) was corrected for the decrease in efficacy of ChR2 at high rates (Barral and Reyes 2016)).

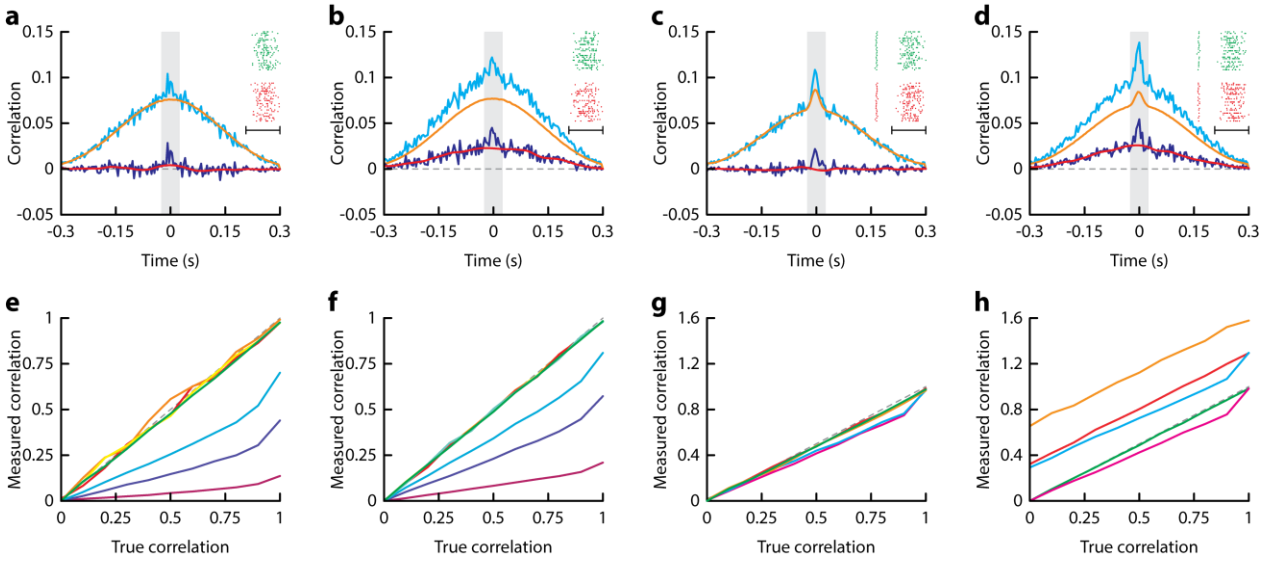

Supplementary Figure 5: Estimation of spike correlation.

a. To build an accurate measure of correlation, we simulated 2 neuronal spike trains where a fixed percentage of spikes were identical in order to vary the correlation in spikes C_{spike} between 0 and 1 (inset; the correlation C_{spike} is here 0.1; scale bar 0.5 seconds). The firing rate was not constant and had a cosine envelop with a maximum rate of 25 Hz. Synchronous and non-synchronous spikes were generated by a Poisson process. Spikes were further randomized with a stochastic jitter of standard deviation 5 ms. From this spike train, we computed the raw cross-correlogram histogram that contains both noise and signal correlations (cyan curve). To isolate the signal correlation only, we cross-correlated each trial of the first neuron with any other trial of the second neuron (orange curve). The subtraction of these two curves gives the noise correlation histogram (dark blue curve). The noise correlation was filtered using a smoothing spline fit (red curve) for which we removed the data points corresponding to an interval of length T_{int} (here T_{int} = 50 ms and is denoted by the grey bar) centered around $t = 0$. The correlation coefficient was calculated as the integral of the area between the noise correlation and the smoothing function in the interval [-0.3 ms, 0.3 ms]. **b.** Same as in **a** but the rate varied on the trial-by-trial basis which resulted in slow timescale noise correlation. The smoothing spline fit allowed eliminating this correlation while keeping the short timescale correlation that we wanted to evaluate. **c.** Same as in **a** but we added a single synchronous spike at the onset of each trial to simulate the experimental data and assess its effect on the correlation measure. This spike resulted in a peak of the signal correlation at short timescale. **d.** Same as in **a** but with the trial-by-trial rate fluctuation and the synchronous spike at the onset. **e.** Measured correlation using the described method with different T_{int} (5, 10, 20, 50, 100, 150, 200 ms, red to purple lines, respectively) as a function of the true correlation C_{spike} for neuronal spike trains generated as in **a**. The grey dotted line denotes the slope of unity. **f.** Same as in **e** but the correlation was simply measured as

the integral of the noise correlation (dark blue curve) in the interval [-0.3 ms, 0.3 ms]. **g.** Measured correlation using the described method with T_{int} = 50 ms as a function of the true correlation C_{spike} for neuronal spike trains generated as in **a** (random spikes with varying C_{spike}; green), as in **b** (random spikes with varying C_{spike} and trial-by-trial rate fluctuations; red), as in **c** (random spikes with varying C_{spike} and the synchronous spike at the onset; magenta), as in **d** (random spikes with varying C_{spike}, trial-by-trial rate fluctuations and the synchronous spike at the onset; cyan), as in **b** but with a larger maximal firing rate of 50 Hz (random spikes with varying C_{spike} and trial-by-trial rate fluctuations; orange). Our measure allowed determining C_{spike} faithfully in every condition. **h.** Same as in **g** but for the simple method described in **f**. This shows that the trial-by-trial rate fluctuations lead to an overestimation of the true correlation and need to be removed.

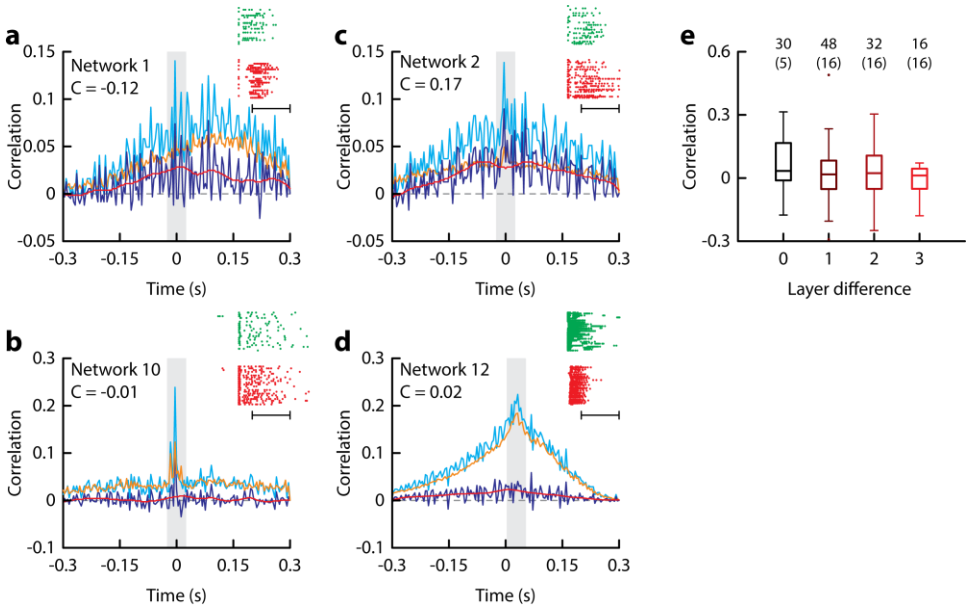

Supplementary Figure 6: Correlation in the feedforward network.

Example of cross-correlogram for neurons recorded in the same layer (**a.-c.**) or in two adjacent layers (**d.**) with the same color code as in Supplementary Figure 5 (raw cross-correlation, cyan; signal correlation, orange; noise correlation, dark blue; filtered noise correlation, red). Spike trains are shown in the inset (scale bar 0.5 seconds). **e.** Spike correlation in dense network as a function of difference in recording layers. Numbers of neuronal pairs are indicated above whisker plots (box: median and interquartile range, whiskers: full range of the distribution; outliers are plotted individually) and numbers of preparations in brackets. No significant difference was found between groups.

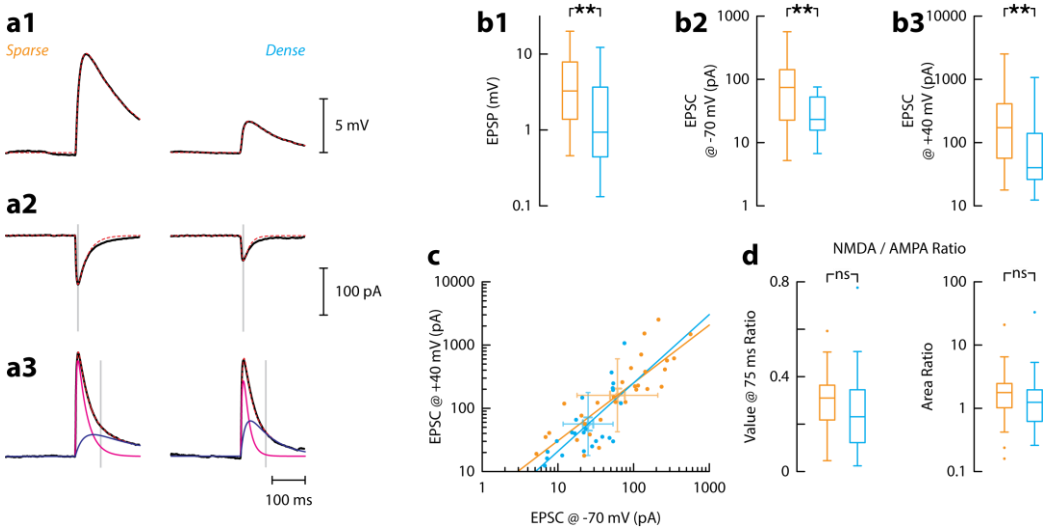

Supplementary Figure 7: NMDA/AMPA ratio in networks of different densities

a. Representative excitatory postsynaptic potential (EPSP, **a1**) and excitatory current recorded at -70 mV ($EPSC_{-70}$, **a2**) or at +40 mV ($EPSC_{+40}$, **a3**) in sparse (left, 202 neurons/mm^2) and dense (right, 920 neurons/mm^2) networks. These experimental traces (black) were fitted by analytical functions (dashed red lines) to determine their peak and areas. EPSPs were fitted by an alpha function. $EPSCs_{-70}$ were fitted by a double exponential function from which we estimated a rise and a decay time. $EPSCs_{+40}$ were fitted by a sum of two double exponential functions using the two characteristic times estimated earlier as fixed parameters (AMPA current shown in magenta and NMDA current shown in dark blue). **b.** EPSP (**b1**), $EPSC_{-70}$ (**b2**), and $EPSC_{+40}$ (**b3**) sizes were measured at the peak and were significantly larger in sparse (orange) than in dense (blue) networks in agreement with previous results (Ivenshitz and Segal 2010, Barral and Reyes 2016). ** P <0.01; EPSP: P = 0.0042; $EPSC_{-70}$: P = 0.0032; $EPSC_{+40}$: P = 0.0044 (n = 30, 306±140 neurons/mm^2 for sparse networks and n = 23, 876±144 neurons/mm^2 for sparse networks). **c.** The size of $EPSC_{-70}$ and $EPSC_{+40}$ were correlated (Pearson correlation coefficient in sparse networks: r = 0.85, p = 3.6×10^{-9}, n = 30; and in dense networks: r = 0.71, p = 1.3×10^{-4}, n = 23) and their slopes were not significantly different from unity (0.91±0.22 and 1.08±0.48 for sparse and dense networks, respectively) suggesting that NMDA and AMPA current varied proportionally. **d.** We used two measures of NMDA/AMPA ratio. *Left*: ratio between the value of $EPSC_{+40}$ at 75 ms after EPSC and the peak value of $EPSC_{-70}$. *Right*: ratio between the area of NMDA current and the AMPA current, both of which were estimated from the fits of $EPSC_{+40}$ (see **a3**). None of these ratios were significantly different (Ratio 1: P = 0.19; Ratio 2: P = 0.40).

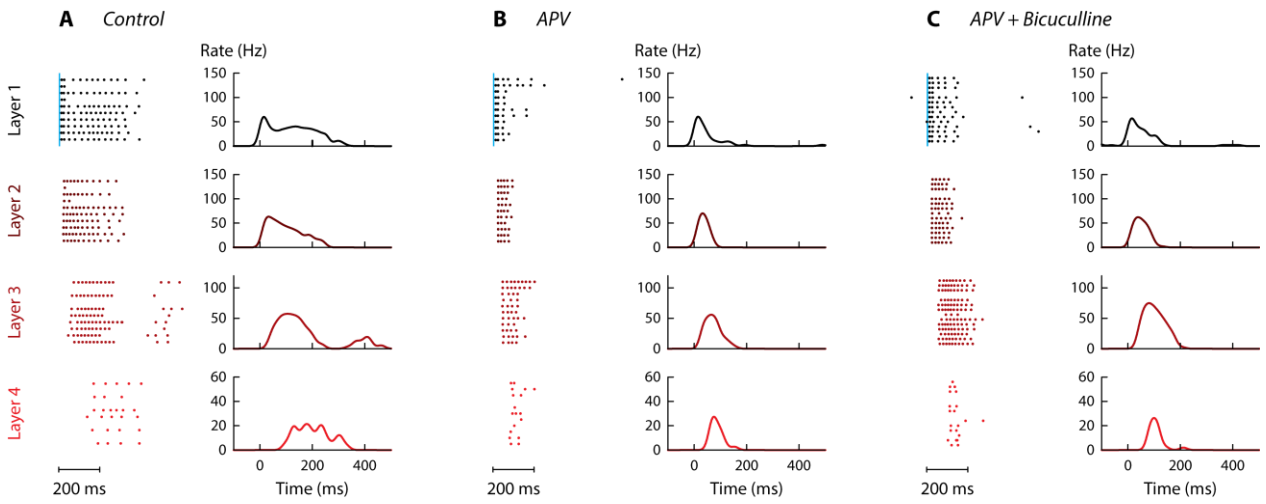

Supplementary Figure 8: Role of AMPA and NMDA synapses in the feedforward propagation

Dot rasters showing spikes recorded from a neuron in each layer in cell attached mode (10-14 repetitions of the light stimuli, left) and corresponding firing rate (right). Results shown for control condition (**A**), with the addition of 50 μM APV (**B**) and with the addition of 50 μM APV and 10 μM bicuculline (**C**).

References

Barral, J. and A. D. Reyes (2016). "Synaptic scaling rule preserves excitatory-inhibitory balance and salient neuronal network dynamics." Nat Neurosci **19**(12): 1690-1696.
Ivenshitz, M. and M. Segal (2010). "Neuronal density determines network connectivity and spontaneous activity in cultured hippocampus." J Neurophysiol **104**(2): 1052-1060.